arXiv:1412.7243v1 [astro-ph.SR] 23 Dec 2014

Can surface oxygen abundances of red giants be explained by the canonical mixing theory?*

Yoichi Takeda,[1,2] Bun'ei Sato,[3] Masashi Omiya,[1] and Hiroki Harakawa[1]

[1] *National Astronomical Observatory, 2-21-1 Osawa, Mitaka, Tokyo 181-8588*

takeda.yoichi@nao.ac.jp

[2] *The Graduate University for Advanced Studies, 2-21-1 Osawa, Mitaka, Tokyo 181-8588*

[3] *Tokyo Institute of Technology, 2-12-1 Ookayama, Meguro-ku, Tokyo 152-8550*

(Received 2014 December 8; accepted 2014 December 18)

Abstract

Extensive oxygen abundance determinations were carried out for 239 late-G/early-K giant stars of 1.5–5 $M_\odot$ by applying the spectrum-fitting technique to O I 7771–5 and [O I] 6300/6363 lines based on the high-dispersion spectra in the red region newly obtained at Okayama Astrophysical Observatory. Our main purpose was to clarify whether any significantly large ($\lesssim$ 0.4–0.5 dex) O-deficit really exists in these evolved stars, which was once suspected by Takeda et al. (2008, PASJ, 60, 781) from the analysis of the [O I] 5577 line, since it (if real) is inexlainable by the current theory and may require the necessity of special non-canonical deep mixing in the envelope. We found, however, that the previous $[O/H]_{5577}$ results (differential abundances relative to the sun) were systematically underestimated compared to the more reliable $[O/H]_{7773}$ (from O I 7771–5 triplet lines) or $[O/H]_{6300}$ (from [O I 6300 line) obtained in this study. Comparing the updated [O/Fe] ratios with the theoretically predicted surface abundance changes caused by mixing of nuclear-processed products dredged-up from the interior, we concluded that the oxygen deficiency in these red giants is insignificantly marginal (only by $\lesssim$0.1 dex), which does not contradict the expectation from the recent theoretical simulation. This consequence of reasonable consistency between theory and observation also applies to the extent of peculiarity in [C/Fe] and [Na/Fe], which were also examined by reanalyzing the previous equivalent-width data of C I 5052/5380 and Na I 6160 lines.

Key words: stars: abundances — stars: atmospheres — stars: evolution — stars: late-type

* Based on data collected at Okayama Astrophysical Observatory of NAOJ (Okayama, Japan).

1. Introduction

Red giants are stars of low-to-intermediate mass, which have already evolved off the main sequence (after the exhaustion of core hydrogen) while increasing their radius. Since the surface temperature progressively drops down according to this evolution, the deep convection zone is developed. As a result, some portion of the H-burning (CNO cycle) product processed in the interior may be salvaged and mixed into the envelope, by which the surface abundances of specific light elements are more or less altered. According to the current theory of envelope mixing, it is primarily the CN-cycled (C→N reaction) material that is dredged up, while the product of ON-cycle (O→N reaction; occurring in deeper region of higher T) is unlikely to cause any significant abundance changes since the mixing does not penetrate into such a deep/hot layer. Thus, the predicted surface abundances are characterized by a deficit in C as well as an enhancement in N (with its peculiarity degree increasing with mass/luminosity), while O is practically unaffected (see, e.g., Fig. 24 in Mishenina et al. 2006). Yet, although such expected tendency has been almost confirmed observationally for C and N, the situation for O seems to remain still more controversial.

For example, Mishenina et al. (2006) found that the oxygen abundances (determined based on the [O I] forbidden line at 6300 Å) in red-clump giants of $\sim$ 1–3 $M_\odot$ are almost normal ($\langle$[O/Fe]$\rangle \simeq 0$), in agreement with the theoretical prediction. Further, Tautvaišienė et al.'s (2010) similar study on red-clump giants resulted in essentially the same conclusion. These results suggest the practical validity of the current mixing theory, in the sense that it satisfactorily explains the behaviors of all C, N, and O.

However, Takeda, Sato, and Murata (2008; hereinafter referred to as Paper I) reported based their extensive spectroscopic analysis of 322 late-G and early-K giants (4500 K $\lesssim T_{\rm eff} \lesssim$ 5500 K, 1.5 $\lesssim \log g \lesssim$ 3.5, 1 $\lesssim M/M_\odot \lesssim$ 5) that [O/Fe] (determined from [O I] 5577 line) showed a subsolar tendency with the extent of peculiarity increasing with M (cf. figure 12 therein). Moreover, this O-deficiency seemed to be correlated with a deficit of C as well as with an overabundance of Na. This may imply that a significant mass-dependent deep dredge-up of (not only CN-cycle but also) ON-cycle products may take place in the envelope of red giants. If this is real, it would possibly require a substantial revision of the current theory for the dredge-up in the envelope of red giants.

One serious concern regarding the consequence in Paper I was, however, that only one weak forbidden [O I] line of $\chi_{\rm low} = 1.97$ eV at 5577 Å (which had been rarely used in previous studies) had to be invoked for the O abundance determination, since only spectra of $\sim$ 5000–6200 Å region were available at that time. As a matter of fact, we noticed based on the comparison with the results of other studies published so far that the oxygen abundances determined from this line do not necessarily agree with those derived from the [O I] 6300 line (most popularly used for O-abundance analyses of red giants) or O I 7771–5 triplet lines (which

were also shown to be a good indicator of oxygen abundances by Takeda et al. 1998), as described in the Appendix of Paper I. Given this situation, we have realized the necessity of reinvestigating the oxygen abundances of red giants by using the presumably more reliable [O I] 6300 (along with similar [O I 6363) and O I 7771–5 lines based on an extensive sample of stars like the case of Paper I.

Motivated by this requirement, we decided to revisit the oxygen problem for red giants based on new observational material obtained for an extensive sample of 239 stars (making up $\sim 3/4$ of all the targets in Paper I), which cover the longer wavelength region (up to ~ 8800 Å) and allowed us to use such O I and [O I] lines mentioned above. In addition, in order to revise the abundances of C and Na (important key elements affected by dredge-up of nuclear-processed products) along with O, the equivalent widths of [O I] 5577, C I 5052/5380, Na I 6160 lines measured in Paper I were also reanalyzed in a more careful manner (e.g., taking into account the CO formation effect or the non-LTE effect), and a new spectrum-fitting analysis was performed for the [C I] 8727 line by using our new spectra. The purpose of this paper is to report the outcome of this analysis.

2. Observational data and stellar parameters

Our spectroscopic observations were done in 2012 August, 2013 May, 2013 August, 2013 November, and 2013 December by using the HIDES (HIgh Dispersion Echelle Spectrograph) placed at the coudé focus of the 188 cm reflector at Okayama Astrophysical Observatory. Equipped with three mosaicked 4K×2K CCD detectors[1] at the camera focus, HIDES enabled us to obtain an echellogram covering 5100–8800 Å (wavelength span of ~ 3700 Å) with a resolving power of $R \sim 67000$ (case for the normal slit width of 200 μm) in the mode of red cross-disperser. While we tried to cover as many stars of the 322 objects studied in Paper I as possible, we could finally get data for 239 stars (about $\sim 3/4$) over these five observing periods.

The reduction of the spectra (bias subtraction, flat-fielding, scattered-light subtraction, spectrum extraction, wavelength calibration, and continuum normalization) was performed by using the "echelle" package of the software IRAF[2] in a standard manner. Since $\sim$ 2–3 consecutive frames (mostly 10–20 min exposure for each) were observed in a night for each star in many cases, we co-added these to improve the signal-to-noise ratio, by which the average S/N of most stars turned out to be in the range of $\sim$ 100–300. Regarding the solar spectrum used as a reference, we adopted the moon spectra observed with HIDES, which were published by Takeda et al. (2005).

[1] Note that, until 2006 when the data used in Paper I were obtained, only one 4K×2K CCD was available and the wavelength coverage was only ~ 1200 Å in HIDES.

[2] IRAF is distributed by the National Optical Astronomy Observatories, which is operated by the Association of Universities for Research in Astronomy, Inc. under cooperative agreement with the National Science Foundation.

Some representative spectra in four wavelength regions comprising our main target lines ([O I] 6300, [O I] 6363,[3] O I 7771–5, and [C I] 8727) are shown in figure 1 for four objects (HD 4627, HD 19476, HD 71369, and the sun).

We remark that the line [O I] 6300 critically falls near to the inter-detector gap. Unfortunately, since our choice of the cross-disperser setting angle was slightly inappropriate due to our mis-adjustment in 2013 August and 2013 November observations, this 6300 line fell just outside of the detector and could not be used for these data (this incident applied to 78 stars out of 239 in total).

Regarding the stellar parameters ($T_{\rm eff}$, $\log g$, [Fe/H], $v_{\rm t}$, M, ...) and the atmospheric model of each star, we exclusively adopted those determined/used in Paper I unchanged. The mutual correlations of the parameters (including the theoretical HR diagram along with the evolutionary tracks) are plotted in figure 2. The basic data of our 239 program stars (HD number, stellar parameters, date of observation) are given in the electronic table E ("tableE.txt").

3. Abundance determination

3.1. Synthetic spectrum fitting

Abundance determinations were carried out by using our spectrum-analysis tool MPFIT, which was developed by Y. Takeda based on Kurucz's (1993a) WIDTH9 code. This program establishes the most optimum solutions accomplishing the best match between theoretical and observed spectra by using the numerical algorithm described in Takeda (1995), while simultaneously varying the abundances of relevant key elements ($\log\epsilon_1$, $\log\epsilon_2$, ...), the macrobroadening parameter ($v_{\rm M}$),[4] and the radial-velocity (wavelength) shift ($\Delta\lambda$).

Specifically, our spectrum fitting was conducted for the following four wavelength regions, 7770–7777 Å [to determine $\log\epsilon$(O) from the O I 7771–5 lines and $\log\phi$(CN) from the CN lines (see the note in table 1 for the meaning of $\log\phi$(CN))], 6300–6302 Å [to determine $\log\epsilon$(O) from the [O I] 6300 line (partially blended with the Ni I 6300 line)], 6362–6365 Å [to determine $\log\epsilon$(O) from the [O I] 6363 line (partially blended with the CN 6363 line)], and 8726–8730 Å [to determine $\log\epsilon$(C) from the [C I] 8727 line partially blended with the Fe I 8727 line], as summarized in table 1. Note that the procedure of analysis for the 7770–7777 Å region was done in essentially the same manner as in Takeda et al. (1998), which should be consulted for more details. Since the O I 7771–5 permitted lines are known to suffer a considerable non-LTE correction (in contrast to other [O I] or [CI] forbidden lines, for which LTE is guaranteed to hold), we explicitly took the non-LTE effect into consideration in the calculation of these triplet

[3] Since this line overlaps the broad and shallow autoionization wing of the Ca I 6361.786 line, the normalization was done by treating this autoionization wing as a pseudo-continuum.

[4] This $v_{\rm M}$ is the e-folding half-width of the Gaussian broadening function ($\propto\exp[-(v/v_{\rm M})^2]$), which represents the combined@effects of instrumental broadening, macroturbulence, and rotational velocity (cf. subsubsection 4.2.2 in Paper I).

lines following Takeda (2003).

The atomic parameters (wavelengths, excitation potentials, oscillator strengths) of important spectral lines adopted in this fitting are presented in table 2. As for the damping parameters (which are unimportant in the present case because very strong lines are absent in the relevant wavelength regions), the data given in Kurucz and Bell (1995) were used; if not available therein, we invoked the default treatment of Kurucz's (1993a) WIDTH9 program.

The convergence of the solutions turned out fairly successful for most of the cases. How the theoretical spectrum for the converged solutions fits well with the observed spectrum for each star is displayed in figure 3 (7770–7777 Å fitting), figure 4 (6300-6302 Å fitting and 6362-6365 Å fitting), and figure 5 (8726–8730 Å fitting).

3.2. Equivalent widths and abundance uncertainties

While the synthetic spectrum fitting directly yielded the abundance solutions of O (and C), this approach is not necessarily suitable when one wants to quantify the contribution of blending components, evaluate the extent of the non-LTE correction, or to study the abundance sensitivity to changing the atmospheric parameters (i.e., it is rather tedious to repeat the fitting process again and again for different assumptions or different atmospheric parameters). Therefore, with the help of Kurucz's (1993a) WIDTH9 program[5], we computed the equivalent widths corresponding to the relevant lines "inversely" from the abundance solutions (resulting from spectrum synthesis) along with the adopted atmospheric models and parameters, which are much easier to handle: $W_{\rm O7771}$, $W_{\rm O7774}$, and $W_{\rm O7775}$ (for O I 7771, 7774, 7775) from $\log\epsilon$(O) of 7771–7777 Å fitting; $W_{\rm O6300}$ and $W_{\rm Ni6300}$ (for [O I] 6300 and Ni I 6300) from $\log\epsilon$(O) and $\log\epsilon$(Ni) of 6300–6302 Å fitting; $W_{\rm O6363}$ and $W_{\rm CN6363}$ (for [O I] 6363 and CN 6363) from $\log\epsilon$(O) and $\log\phi$(CN) of 6362–6365 Å fitting; $W_{\rm C8727}$ and $W_{\rm Fe8727}$ (for [C I] 8727 and Fe I 8727) from $\log\epsilon$(C) and $\log\epsilon$(Fe) of 8726–8730 Å fitting. Regarding the O I 7771, 7774, 7775 lines, the non-LTE as well as LTE abundances were also derived based on such evaluated W values, from which the non-LTE corrections ($\Delta^{\rm NLTE}_{7771}$, $\Delta^{\rm NLTE}_{7774}$, $\Delta^{\rm NLTE}_{7775}$) were computed. The results of the abundances,[6] the equivalent widths (W), and the non-LTE corrections ($\Delta^{\rm NLTE}$) are summarized in the on-line table E ("tableE.txt"). Besides, such derived W values (along with the related quantities) for the relevant lines are plotted against $T_{\rm eff}$ and [Fe/H] in figure 6, from which we can realize the relative importance of the contribution of blended lines as compared to the O and C lines of our interest.

Regarding the abundance errors due to ambiguities in atmospheric parameters, we estimated the changes in $\log\epsilon$(O) and $\log\epsilon$(C) by repeating the analysis on the W value of each

[5] This WIDTH9 program had been considerably modified in various respects; e.g., inclusion of non-LTE effects, treatment of total equivalent width for multi-component lines; etc.

[6] Abundances are given in $\log\epsilon$(X) as well as in [X/H], where $\log\epsilon$(X) is the logarithmic abundance of element X in the usual normalization of $\log\epsilon$(H) = 12, and [X/H] is the differential abundances relative to the Sun defined as $[{\rm X/H}] \equiv \log\epsilon_*({\rm X}) - \log\epsilon_\odot({\rm X})$.

line ($W_{\rm O7774}$, $W_{\rm O6300}$, $W_{\rm O6363}$, $W_{\rm C8727}$) while perturbing the standard atmospheric parameters interchangeably by $\pm$100 K in $T_{\rm eff}$, $\pm$0.2 dex in $\log g$, and $\pm$0.2 km s^{-1} in ξ (which are considered to be typical magnitudes of ambiguities; see subsection 3.1 in Paper I, especially the comparison with the literature values shown in figures 5–7 therein). The resulting abundance changes are summarized in table 3, from which the following tendencies are read.

— The $T_{\rm eff}$-sensitivity of O I 7771–5 lines is appreciably large ($\lesssim$0.2 dex for a change of 100 K), while that of forbidden lines is insignificant (much smaller for [C I] 8727 and negligible for [O I] 6300/6363).

— Regarding the effect of changing $\log g$, all these lines show almost the same behaviors of mild sensitivity ($\sim$0.1 dex for a change of 0.2 dex).

— Abundances are practically unaffected by a change in $v_{\rm t}$ ($\sim$ 0.02 dex for O I 7771–5 or a few hundredths dex for forbidden lines[7] in response to a variation of 0.2 km s^{-1}).

3.3. Reanalysis of C, O, and Na equivalent widths in Paper I

While C, O, and Na abundances were determined for 322 giants from the equivalent widths of C I 5052/5380, [O I] 5577, and Na I 6160 lines in Paper I, the treatment adopted there was not necessarily full-fledged. More precisely, no consideration was made to the non-LTE effect as well as the molecule-formation effect, they are not quantitatively significant for these lines and tend to be more or less cancelled in [X/H] (differential abundances relative to the Sun). However, attention should be paid also to these effects (which generally differ from star to star) to accomplish as accurate [X/H] values as possible. Accordingly, we decided to reanalyze the equivalent widths (W) for these lines (published in Paper I) while taking these factors explicitly into account (as we have done in our main analysis described in subsection 3.1), in order to revise $[{\rm C/H}]_{5052/5380}$, $[{\rm O/H}]_{5577}$, and $[{\rm Na/H}]_{6160}$ for our 239 program stars.

Computing populations by including molecules (where the formation of CO is especially important) was done by following the treatment used in Kurucz's (1993) ATLAS9 program. Meanwhile, the non-LTE corrections were evaluated as done in Takeda and Honda (2005) for C and Takeda et al. (2003) for Na (while LTE is essentially valid for the [O I] 5577 forbidden line). The resulting non-LTE corrections are plotted against W in figures 7a (C I 5052), 7b (C I 5380), and 7c (Na I 6160), where the tendency of increasing $|\Delta^{\rm NLTE}|$ with an increase in W is seen. Since the extents of (negative) non-LTE corrections for red giants are generally larger than that for the sun (reflecting the nature of lower-density atmospheres), [C/H] as well as [Na/H] have been corrected in the downward direction as shown figures 7d and 7f, though the corrections ($\lesssim$ 0.1 dex) are quantitatively not very important. On the other hand, since $\log \epsilon$(O) derived

[7] Regarding the [C I] 8727 forbidden line, the sign of the abundance change in response to varying $v_{\rm t}$ is contrary to what is intuitively expected (i.e., the resulting abundance slightly increases for a larger $v_{\rm t}$). This phenomenon is sometimes seen in case of very weak lines of light elements, which may be interpreted as due to the difference of photon-forming layers at different points of line profiles (see subsection 3.2 in Takeda 1994).

from [O I] 5577 line tends to be somewhat increased by including CO formation effect (which is more appreciable for lower-$T_{\rm eff}$ stars), $[{\rm O/H}]_{5577}$ values have been revised in the upward direction for stars with $T_{\rm eff} \lesssim 5000$ K (cf. figure 7e), though these corrections ($\lesssim 0.06$ dex) are again not so significant. These updated results for $[{\rm C/H}]_{5052/5380}$ (which is the average of $[{\rm C/H}]_{5052}$ and $[{\rm C/H}]_{5380}$), $[{\rm O/H}]_{5577}$, and $[{\rm Na/H}]_{6160}$ are also summarized in electronic table E (tableE.txt).

4. Discussion

4.1. Comparison of the abundances from different lines

We have thus derived the oxygen abundances for the program stars by applying the spectrum-fitting technique to three line features: O I 7771–5, [O I] 6300, and [O I] 6363 lines (subsection 3.1). How are they compared with each other, and how do they relate to the results from O I 5577 (subsection 3.3) derived by reanalyzing the W values of Paper I? Which abundance indicator is most reliable?

The mutual comparisons of these [O/H] values are depicted in figures 8a–8f, in which we can recognize that a tendency $[{\rm O/H}]_{5577} \lesssim [{\rm O/H}]_{6363} < [{\rm O/H}]_{6300} \simeq [{\rm O/H}]_{7773}$ roughly holds. That is, a reasonable consistency is observed between $[{\rm O/H}]_{7773}$ and $[{\rm O/H}]_{6300}$ (cf. figure 8d), while $[{\rm O/H}]_{6363}$ and (especially) $[{\rm O/H}]_{5577}$ are systematically lower than these two.

We consider that the O I 7771–5 feature is the most reliable abundance indicator among these in the present case of red giants, given that the spectrum-synthesis technique is applied and the non-LTE effect (rather appreciable; cf. figure 6b) is properly taken into account, because it comprises three components of different strengths and the blending effect by other lines is insignificant. That is, we may regard that the resulting abundance is reliable if the whole triplet feature could be adequately fitted by theoretically synthesized spectrum, even though its large $T_{\rm eff}$-sensitivity (cf. subsection 3.2) may be a drawback.

Regarding the forbidden lines [O I] 6300 and [O I] 6363, they are often used for O-abundance determination of red giants, since they get strengthened in lower-g atmospheres and formed essentially in LTE. We consider, however, that their credibility would be comparatively lower, because only one [O I] line component is blended by line(s) of other species and the removal of this effect inevitably causes loss of accuracy. The contamination is especially significant for the [O I] 6363.78 line which is overlapped by the CN 6363.78 line. Actually, the contribution of this CN line can be appreciable (typically several tens per cent or even more up to a comparable level; cf. figure 6e and figure 6h). Moderately enhanced CN population by up to $\lesssim 0.4$ dex (see figure 6c) may also be partly responsible for this fact, which is a combined result of considerably increased N and mildly decreased C in the atmosphere of red giants (see, e.g., Mishenina et al. 2006). Meanwhile, concerning the [O I] 6300.30, we can see from figure 6d and figure 6g that the contribution of the blending Ni I 6300.35 line is not very significant

compared to the case of [O I] 6363.

Given these results, it is reasonable to state that O I 7771–5 and [O I] 6300 lines are the reliable abundance indicators in the present case, and thus we should adopt the O abundances derived from these two features (which are mostly in agreement as shown in figure 8d).

4.2. Problem involved with the [O I] 5577 line

This judgement naturally leads to a conclusion that $[O/H]_{5577}$ values are erroneously inadequate, since they are systematically smaller than $[O/H]_{7773}$ (figure 8e) and $[O/H]_{6300}$ (figure 8a). Actually, this possibility was already suspected in Paper I (cf. Appendix therein); but at that time we could not find a reason why this [O I] 5577 line yielded wrong differential oxygen abundances relative to the sun.

After Paper I has been published, however, we noticed Meléndez and Asplund's (2008) work, who studied the solar oxygen abundance based on the [O I] 5577 line by using a 3D model atmosphere. We realized from their paper that this [O I] feature is contaminated by $P_1 27$ and $P_1 26$ lines of C_2 (1–2) Swan band (cf. their Fig. 2), the blending effect of which needs to be taken into account.

We tried to estimate how much contribution is made by these C_2 lines to the strength of the [O I] 5577 feature. Since these two lines are almost the same strength ($P_1 27$ is at 5577.338 Å with $\chi_{\rm low} = 0.726$ eV and $\log gf = 1.364$, $P_1 26$ is at 5577.404 Å with $\chi_{\rm low} = 0.727$ eV and $\log gf = 1.381$) according to Kurucz's (1993b) molecular line data (c2da.dat), we may tentatively focus only on the former 5577.338 line. Regarding the [O I] line, the same atomic data as used in Paper I was adopted (5577.339 Å, $\chi_{\rm low} = 1.967$ eV and $\log gf = -8.204$). We computed the equivalent widths of these lines ([O I 5577.339 and C_2 5577.338) for the sun and a typical red giant ($T_{\rm eff} = 4900$ K, $\log g = 2.5$, and [Fe/H] = 0) on the assumption of [C/H] = 0, and obtained (1.69 mÅ and 0.75 mÅ) for the sun and (7.40 mÅ and 2.95 mÅ) for a red giant.

It might appear that the relative contribution of C_2 blending is almost the same for the sun and red giant and cancelled in the net differential abundances, since the resulting W(O):W(C_2) ratios are practically identical as 1.7:1.5(= 2×0.75) and 7.4:5.9(= 2×2.95), However, we should keep in mind that C is generally deficient in the atmosphere of red giants typically by 0.2–0.3 dex (cf. figure 11a and figure 11b) by mixing of CN-cycled products. As the population of C_2 molecules scales as $n(C_2) \propto \epsilon(C)^2$, the contribution of C_2 lines to the 5577 feature must be further reduced by a factor of $\sim$ 3–4 to an insignificant level compared with the [O I] line itself.

Thus, our interpretation for the reason why we obtained erroneously low $[O/H]_{5577}$ values is simply that we did not take into account the blending effect of two C_2 lines in our analysis; its influence was not so significant for red giants but serious for the sun (standard star). That is, since the reference solar O abundance was overestimated by ~ 0.3 dex by neglecting this

effect in the analysis of the [O I] (+ C_2) line feature at 5577 Å (while the extent of such an overestimation is much milder or even negligible for giant stars), we eventually obtained systematically underestimated $[O/H]_{5577}$ in comparison to (presumably correct) $[O/H]_{7773}$ or $[O/H]_{6300}$.

4.3. Correlation between [O/Fe], [C/Fe], and [Na/Fe]

Let us examine based on the revised abundances how O, C, and Na are correlated with each other, and how the situation is changed compared to what was concluded in Paper I. We adopt the oxygen abundances derived from O I 7771–5 and [O I] 6300 lines according to the discussion in subsection 4.1, while the non-LTE abundances obtained by reanalyzing the W(Na I 6161) data are used for Na (subsection 3.2).

Regarding C, although the abundances from the [C I] 8727 forbidden line were newly determined in this study, they suffer from appreciable contamination of the overlapping Fe I line (cf. figure 6f and figure 6i), and considered to be less reliable. Since the consistency between the [C/H] values derived from [C I] 8727 and those from C I 5052/5380 is not necessarily satisfactory (i.e., rather large scatter with some systematic difference; cf. figure 8g), we put larger weight to the latter non-LTE abundances obtained by reanalyzing the W(C I 5052) and W(C I 5380) data (subsection 3.2), where the results derived from these two permitted C I lines were averaged since they are in agreement with each other (figure 8h).

The mutual correlations between [O/Fe], [C/Fe], and [Na/Fe], and their dependence upon [Fe/H] as well as M are depicted in figure 9. Comparing figure 9a ([O/Fe] vs. [C/Fe]), figure 9b ([Na/Fe] vs. [C/Fe]), and figure 9c ([Na/Fe] vs. [O/Fe]) with the corresponding figures in Paper I (figures 12a, 12b, and 12c therein), we can see that only [O/Fe] values have been appreciably shifted upward by ~ 0.3 dex on the average (due to the use of O I 7771–5 and [O I] 6300 lines in this study instead of the [O I] 5577 line in our previous work), while no significant changes are seen in [C/Fe] as well as in [Na/Fe]. That is, oxygen does not show remarkable deficiency any more, as seen from the range of $-0.2 \lesssim$ [O/Fe] $\lesssim +0.5$ (in contrast to the previous $-0.5 \lesssim$ [O/Fe] $\lesssim +0.2$).

The reason why we suspected in Paper I the existence of non-canonical mixing was that the O-deficiency appeared to conform to the C-deficiency as well as to the Na-enrichment, and the extent of this peculiarity seemed to increase with the stellar mass (cf. figure 12 therein). We thus consider at that time that these characteristics may indicate a deep dredge-up of H-burning (ON-, CN-, NeNa-cycle) products.

However, now that the revised results for O, C, and Na are established, we can reasonably interpret the abundance trends of these elements as follows.

— The positive correlation between [O/Fe] and [C/Fe] is simply due to the α-element-like behavior (i.e., [X/Fe] decreases with an increase in [Fe/H]) shown by these elements (cf. figure 9d and figure 9e), which results from the galactic chemical evolution as exhibited by nearby

solar-type stars (see, e.g., Takeda & Honda 2005).
— The inversed correlation between Na and O (i.e., [Na/Fe] tends to increase with a decrease in [O/Fe]; figure 9c) is mostly attributed to the "upturn" nature of [Na/Fe] with an increase of [Fe/H], which contrasts the trend of O. That is, the different behavior of [O/Fe] (figure 9d) and [Na/Fe] (figure 9f) against a change of [Fe/H] is the cause of this anti-correlation.
— The apparent variation of [O/Fe] against the stellar mass reported in Paper I ([O/Fe] ~ 0 at $M \sim 1$–2 $M_\odot$ and [O/Fe] ~ -0.4 at $M \sim 3$–4 $M_\odot$) has been updated to [O/Fe] ~ 0.4–0.5 at $M \sim 1$–2 $M_\odot$ and [O/Fe] ~ 0 at $M \sim 3$–4 $M_\odot$ by the upward revision of [O/Fe], which thus can not be regarded as a M-dependence of O-deficiency any more. This trend is simply due to the fact that low-M stars tend to have low [Fe/H] (cf. figure 2f), where [O/Fe] is generally enhanced up to $\sim +0.4$–0.5 (figure 9d).

Accordingly, since we have significantly revised the [O/Fe] ratios for the program stars in this study, which are systematically higher (typically by ~ 0.3–0.4 dex) than the values reported in Paper I, we came to a conclusion that the oxygen abundances in red giants atmospheres do not show appreciable peculiarities and that the observed relations between [O/Fe], [C/Fe], and [Na/Fe] can be reasonably explained mostly by their intrinsic qualitative characteristics caused by galactic chemical evolution, without invoking any special a-posteriori mechanism (e.g., non-canonical deep mixing) such that generating a significant O-abundance anomaly.

4.4. Does theoretical predictions explain the observed abundance trends?

Now, we return to the subject which motivated this investigation: "Are the surface oxygen abundances of red giants consistent with the prediction from the canonical theory of envelope mixing? How about carbon and sodium?" In order to answer this question, we have to carefully evaluate the changes in the surface abundances of these elements, which were caused by a mixing of nuclear-processed materials dredged-up in the red-giant stage. For this purpose, it is necessary to adequately take into account the chemical evolution effect (i.e., intrinsic [X/Fe] ratio of the gas at the time of star formation), which can be done by comparing the abundances of evolved red giants with those of unevolved dwarfs at the same metallicity.

In this discussion, we confine ourselves to the abundance results of red giants derived from permitted lines, which we consider to be most reliable: C abundances from C I 5052/5380 lines, O abundances from O I 7771–5 lines, and Na abundances from Na I 6160 line. In addition, we also refer to the C, O, and Na abundances of FGK dwarfs (or subgiants) derived from the same lines, which were taken from Takeda and Honda (2005) (for C and O) as well as Takeda (2007) (for Na).

The [X/Fe] vs. [Fe/H] diagrams (X = C, O, and Na) plotted for giants and dwarfs are shown in the left-side panels (a, b, and c) of figure 10, where the mean $\langle$[X/Fe]$\rangle$ at each metallicity group (0.1 dex bin within $-0.4 \leq$ [Fe/H] $\leq +0.2$) along with the distribution of $\langle$[X/Fe]$\rangle_{\rm giants} - \langle$[X/Fe]$\rangle_{\rm dwarfs}$ are also presented in the corresponding right-side panels (d, e,

and f). We can state from figure 10d, 10e, and 10f that the abundance changes (compared to the initial values when stars were formed) suffered in the red-giant phase by evolution-induced envelope mixing are a moderate decrease of C by ~ 0.2 dex, only a slight decrease of O by $\lesssim 0.1$ dex, and a marginal increase of Na by ~ 0.1–0.2 dex.

Then, what about the theoretically predicted abundance anomalies of low-to-intermediate mass stars in the red giant phase? In figure 11 are shown the expected surface abundance changes of C, O, and Na during the course of post-main-sequence stellar evolution (plotted against $T_{\rm eff}$) calculated by Lagarde et al. (2012) for 1.5, 2.5, and 4 $M_{\odot}$ stars, where the results for different assumptions of envelope mixing (standard treatment and treatment including rotational and thermohaline mixing)[8] are presented for two metallicity cases ($0.3\times$ solar metallicity and $1\times$ solar metallicity). Although it is difficult to confront these results in detail with the observations as the computed anomalies intricately depend on various factors (mass, metallicity, assumptions on mixing), we can draw the following consequences from the comparison of figure 10 and figure 11:

— Regarding oxygen, our observational result (only a slight deficiency by $\lesssim 0.1$ dex) satisfactorily matches the theoretical expectation that the surface O abundances are hardly altered (the predicted decrease is $\lesssim 0.05$ dex at most). This means that the current theory for the mixing in the envelope of evolved stars is quite sufficient to account for the observed oxygen abundances of red giants, without any necessity to invoke a non-canonical deep mixing causing a significant dredge-up of ON-cycle product.

— The observed mild enrichment of Na and deficiency of C are reasonably predicted by the simulations. That is, if we consider the typical case of a 2.5 $M_{\odot}$ star of solar-metallicity around $T_{\rm eff} \sim 4800$–5000 K, figure 11a$'$ and figure 11c$'$ suggest that the expected abundance changes are an underabundance of C by ~ 0.2–0.3 dex and an overabundance of Na by ~ 0.2–0.3 dex. Though the observed extents of anomaly (~ 0.2 dex deficiency for C and ~ 0.1–0.2 dex enrichment for Na) appear somewhat smaller than the theoretical predictions (e.g., the case of Na), we may state that theory and observation are tolerably consistent with each other.

Consequently, according to what has been described above, the abundance characteristics of C (mildly deficient), O (barely changed or only slightly deficient), and Na (mildly enriched) observed in red giants are reasonably explained by the recent theoretical simulation such as that by Lagarde et al. (2012). This consistency indicates that a substantial or intrinsic modification of the theory (such as an inclusion of special non-canonical deep mixing) is not necessary, though some refinements on technical details in simulations (e.g., which kind of physical processes are to be included in the envelope mixing) will naturally be further in order.

[8] We consider that rotational/thermohaline mixing actually takes place in addition to the standard mixing of first dredge-up, according to Takeda and Tajitsu's (2014) recent study on the Be abundances of red giants.

5. Summary and conclusion

Takeda et al. (2008) suggested in Paper I based the analysis of the [O I] 5577 line carried out for 322 late G–early K giants that oxygen is significantly underabundant in their atmospheres. If this is real, it might suggest a dredge-up of ON-cycle product caused by a non-canonical deep-mixing, such as that unable to be covered by the current theory.

However, this result apparently contradicted the consequence of other studies (e.g., Mishenina et al. 2006, Tautvaišienė et al. 2010), which concluded based on the [O I] 6300 line that O is almost normal (without any sign of significant anomaly) in the atmosphere of red giants in agreement with the theoretical prediction.

In order to settle this issue by clarifying which conclusion represents the truth, extensive abundance determinations were conducted for oxygen (along with carbon and sodium) for 239 late-G/early-K giant stars by using various lines. We applied the spectrum-fitting technique to O I 7771–5, [O I] 6300/6363, and [C I] 8727 lines to the red-region spectra newly obtained at Okayama Astrophysical Observatory, and reanalyzed the previously published equivalent widths of [O I] 5577, C I 5052/5380 and Na I 6160 lines.

It then revealed that the previous $[O/H]_{5577}$ results in Paper I were systematically underestimated compared to the more reliable $[O/H]_{7773}$ (from O I 7771–5 triplet lines) or $[O/H]_{6300}$ (from [O I] 6300 line) newly obtained in this study. Regarding the reason why [O I] 5577 line yielded erroneously low [O/H], we consider that this was due to our neglect of the blending effect of C_2 lines in deriving the reference solar O abundance from this line.

According to our updated results, the oxygen deficiency of these red giants is actually very marginal (only by $\lesssim 0.1$ dex), which is in good agreement with the expectation from the recent theoretical simulation by Lagarde et al. (2012). The same conclusion also applies to the observed extents in the abundance anomalies of C (~ 0.2 dex deficit) as well as Na (~ 0.1–0.2 dex enrichment) derived from C I 5052/5380 and Na I 6160 lines.

To sum up, the current theoretical simulations are considered to be successful enough in predicting the surface abundance changes of red giants, without any need of substantial revision (such as by incorporating an unreasonably deep mixing process) as far as O, C, and Na are concerned.

Finally, the fact that the atmospheric abundance of oxygen suffers little change even in the evolved giant stage would have a significant impact in observational studies of galactic chemical evolution, since it means that intrinsically bright red giants may be exploited as a tracer of [O/Fe] ratio of the galactic gas at the time of star formation.

Data reduction was in part carried out by using the common-use data analysis computer system at the Astronomy Data Center (ADC) of the National Astronomical Observatory of Japan.

References

Eriksson, K., & Toft, S. C. 1979, A&A, 71, 178

Galavís, M. E., Mendoza, C., & Zeippen, C. J. 1997, A&AS, 123, 159

Kurucz, R. L. 1993a, Kurucz CD-ROM, No. 13 (Harvard-Smithsonian Center for Astrophysics)

Kurucz, R. L. 1993b, Kurucz CD-ROM, No. 18 (Harvard-Smithsonian Center for Astrophysics)

Kurucz, R. L., & Bell, B. 1995, Kurucz CD-ROM, No. 23 (Harvard-Smithsonian Center for Astrophysics)

Lagarde, N., Decressin, T., Charbonnel, C., Eggenberger, P., Ekström, S., & Palacios, A. 2012, A&A 543, A108

Lejeune, T., & Schaerer, D. 2001, A&A, 366, 538

Meléndez, J., & Asplund, M. 2008, A&A, 490, 817

Mishenina, T. V., Bienaymé, O., Gorbaneva, T. I., Charbonnel, C., Soubiran, C., Korotin, S. A., & Kovtyukh, V. V. 2006, A&A, 456, 1109

Takeda, Y. 1994, PASJ, 46, 53

Takeda, Y. 1995, PASJ, 47, 287

Takeda, Y. 2003, A&A, 402, 343

Takeda, Y. 2007, PASJ, 59, 335

Takeda, Y., et al. ,2005, PASJ, 57, 13

Takeda, Y., & Honda, S. 2005, PASJ, 57, 65

Takeda, Y., Kawanomoto, S., & Sadakane, K. 1998, PASJ, 50, 97

Takeda, Y., Sato, B., & Murata, D. 2008, PASJ, 60, 781 (Paper I)

Takeda, Y., & Tajitsu, A. 2014, PASJ, 66, 91

Takeda Y., Zhao G., Takada-Hidai M., Chen Y.-Q., Saito Y.-J., & Zhang H.-W., 2003, ChJAA, 3, 316

Tautvaišienė, G., Edvardsson, B., Puzeras, E., Barisevičius, G., & Ilyin, I. 2010, MNRAS, 409, 1213

Table 1. Treatment of relevant elemental abundances in the fitting.

Abundance	LTE/NLTE	var/fix	Remark
		(7770–7777 Å fitting)	
$\log\epsilon$(O)	non-LTE	varied	
$\log\epsilon$(Fe)	LTE	varied	
$\log\epsilon$(Nd)	LTE	varied	
$\log\phi$(CN)	LTE	varied	
		(6300–6302 Å fitting)	
$\log\epsilon$(O)	LTE	varied	
$\log\epsilon$(Sc)	LTE	varied	
$\log\epsilon$(Fe)	LTE	varied	
$\log\epsilon$(Ni)	LTE	*fixed*	Taken from Paper I
		(6362–6365 Å fitting)	
$\log\epsilon$(O)	LTE	varied	
$\log\epsilon$(Fe)	LTE	varied	
$\log\epsilon$(Zn)	LTE	varied	
$\log\phi$(CN)	LTE	*fixed*	Taken from 7770–7777 Å fitting)
		(8726–8730 Å fitting)	
$\log\epsilon$(C)	LTE	varied	
$\log\epsilon$(Si)	LTE	varied	
$\log\epsilon$(Fe)	LTE	varied	

Note. The quantity ϕ(CN) introduced in the fitting of 7770–7777 Å and 6362–6365 Å regions is a depth-independent factor, by which the occupation numbers of CN molecules (computed from a model atmosphere with metallicity-scaled CNO abundances) are to be multiplied to reproduce the observed CN line strengths (cf. subsection 3.3 in Takeda et al. 1998).

Table 2. Atomic data of important spectral lines.

Species	$\lambda_{\rm air}$ (Å)	$\chi_{\rm low}$ (eV)	$\log gf$ (dex)	Source
		(7770–7777 Å fitting)		
O I	7771.944	9.146	+0.32	KB95
O I	7774.166	9.146	+0.17	KB95
O I	7775.388	9.146	−0.05	KB95
Fe I	7770.279	2.559	−5.12	TKS98
Fe I	7771.427	5.105	−2.48	TKS98
Fe I	7772.597	5.067	−2.16	TKS98
Fe I	7774.001	5.012	−2.27	TKS98
Nd II	7773.052	0.000	−3.38	KB95
CN	7770.76	1.18	−2.01	ET79
CN	7772.88	1.28	−1.72	ET79
CN	7772.95	1.31	−2.19	ET79
CN	7775.42	1.16	−2.10	ET79
CN	7776.68	1.36	−1.64	ET79
CN	7776.69	1.13	−2.45	ET79
		(6300–6302 Å fitting)		
[O I]	6300.304	0.000	−9.72	GA97
Ni I	6300.336	4.266	−2.43	TH05
Sc II	6300.67	1.507	−1.84	KB95 (wavelength adjusted)
Fe I	6301.498	3.654	−0.75	KB95
		(6362–6365 Å fitting)		
Zn I	6362.338	5.796	+0.15	KB95
Fe I	6362.885	4.186	−1.70	This study (gf adjusted)
[O I]	6363.776	0.020	−10.19	GA97
CN	6363.776	1.390	−1.75	KZ93
Fe I	6364.360	4.795	−1.10	This study (gf adjusted)
Fe I	6364.701	4.584	−1.92	This study (gf adjusted)
		(8726–8730 Å fitting)		
[C I]	8727.126	1.264	−8.21	KB95
Fe I	8727.132	4.186	−3.93	KB95
Si I	8728.010	6.181	−0.61	KB95
Si I	8728.594	6.181	−1.72	KB95
Fe I	8729.148	3.415	−2.95	KB95

Abbreviation code for the source of gf values: KB95 — Kurucz and Bell (1995), TKS98 — Takeda et al. (1998), ET79 — Eriksson and Toft (1979), GA97 — Galavís et al. (1997), TH05 — Takeda and Honda (2005), KZ93 — Kurucz (1993b).

Table 3. Abundance variations in response to changing atmospheric parameters.

Line	Δ_{T+}	Δ_{T-}	Δ_{g+}	Δ_{g-}	Δ_{v+}	Δ_{v-}
O I 7774	−0.166 (0.012)	+0.182 (0.015)	+0.090 (0.006)	−0.091 (0.005)	−0.021 (0.008)	+0.020 (0.008)
[O I] 6300	−0.005 (0.006)	+0.006 (0.004)	+0.096 (0.002)	−0.097 (0.002)	−0.004 (0.001)	+0.003 (0.002)
[O I] 6363	−0.005 (0.007)	+0.006 (0.006)	+0.096 (0.003)	−0.096 (0.003)	−0.001 (0.001)	+0.001 (0.001)
[C I] 8727	−0.067 (0.020)	+0.081 (0.021)	+0.116 (0.008)	−0.114 (0.008)	+0.003 (0.002)	−0.006 (0.003)

Note. Changes of the abundances (expressed in dex) derived from each line in response to varying $T_{\rm eff}$ by ±100 K, $\log g$ by ±0.2 dex, and $v_{\rm t}$ by ±0.2 km s^{-1}. Shown are the mean values averaged over each of the 239 stars, while those in parentheses are the standard deviations.

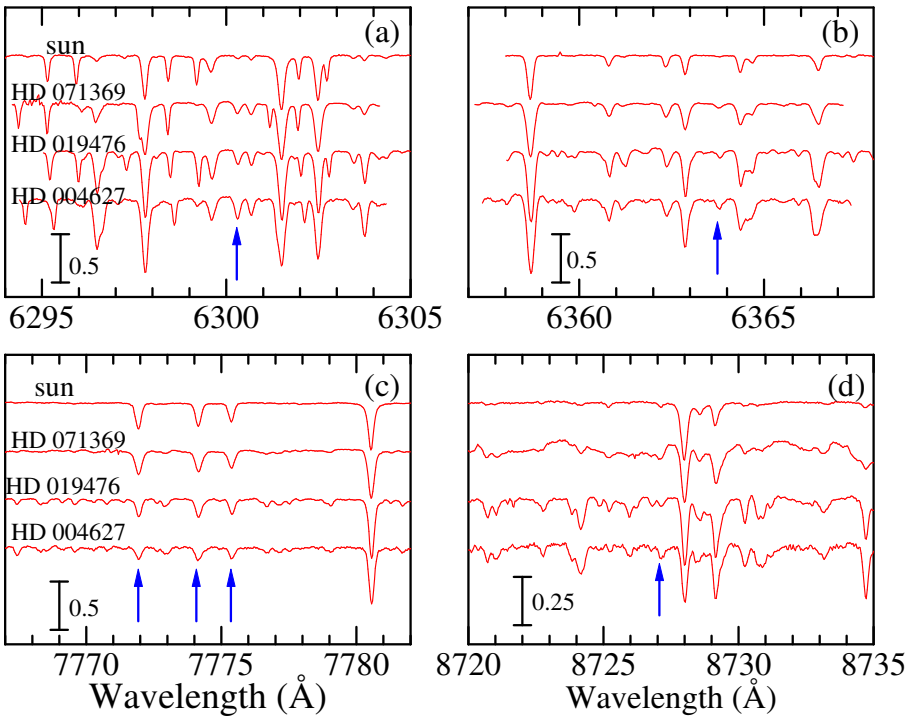

Fig. 1. Representative spectra of three stars selected from our sample (HD 71369, HD 19476, and HD 4627 with different $T_{\rm eff}$ of 5242 K, 4933 K, and 4599 K, respectively) and the sun (moon) for the four wavelength regions comprising the lines used for our abundance determinations: (a) ⋯ [O I] 6300, (b) ⋯ [O I] 6363, (c) ⋯ O I 7771–5, and (d) ⋯ [C I] 8727; which are indicated by arrows in each panel. Note that the ordinate scale of panel (d) is twice as magnified as that of the other panels.

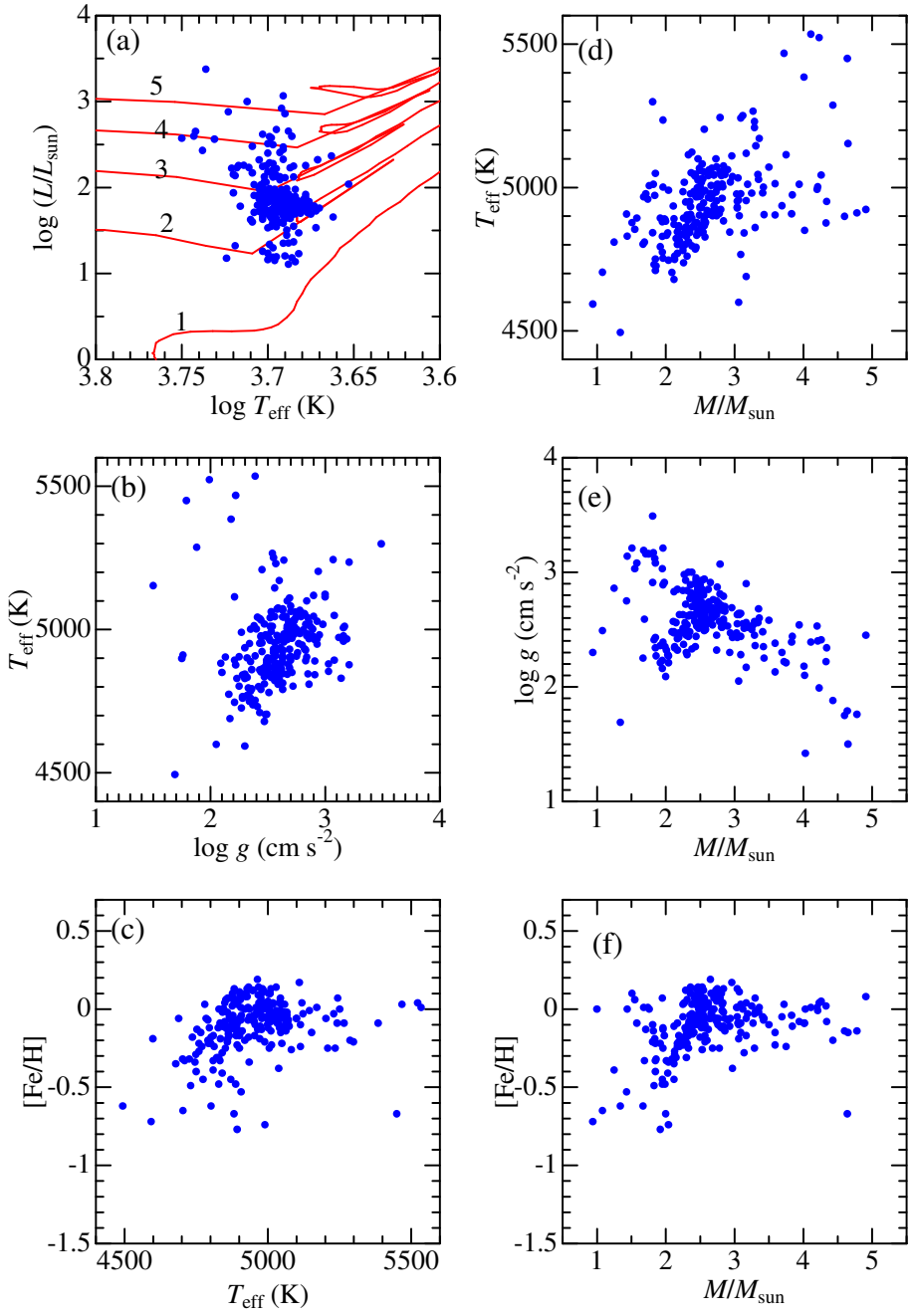

Fig. 2. Mutual correlations between the parameters of 239 program stars. (a) $\log L$ vs. $\log T_{\rm eff}$, (b) $T_{\rm eff}$ vs. $\log g$, (c) [Fe/H] vs. $T_{\rm eff}$, (d) $T_{\rm eff}$ vs. M, (e) $\log g$ vs. M, and (f) [Fe/H] vs. M. In panel (a), Lejeune and Schaerer's (2001) theoretical evolutionary tracks of solar-metallicity stars (with masses of 1, 2, 3, 4, and 5 $M_{\odot}$) are also overplotted.

Fig. 3. Synthetic spectrum fitting in the 7770–7777 Å region comprising the O I 7771–5 triplet lines. The best-fit theoretical spectra are shown by blue solid lines, and the observed data are plotted by red open circles (while those masked/disregarded in the fitting are highlighted in green). A vertical offset of 0.2 (in terms of the normalized flux with respect to the continuum) is applied to each relative to the adjacent ones. Each of the spectra are arranged in the increasing order of HD number (indicated on the left to each spectrum). The wavelength scale of each spectrum is adjusted to the laboratory system.

Fig. 4. Synthetic spectrum fitting in the 6300–6302 Å region comprising the [O I] (+ NiI) 6300 line as well as in the 6362–6365 Å region comprising the [O I] (+ CN) 6363 line. Otherwise, the same as in figure 3.

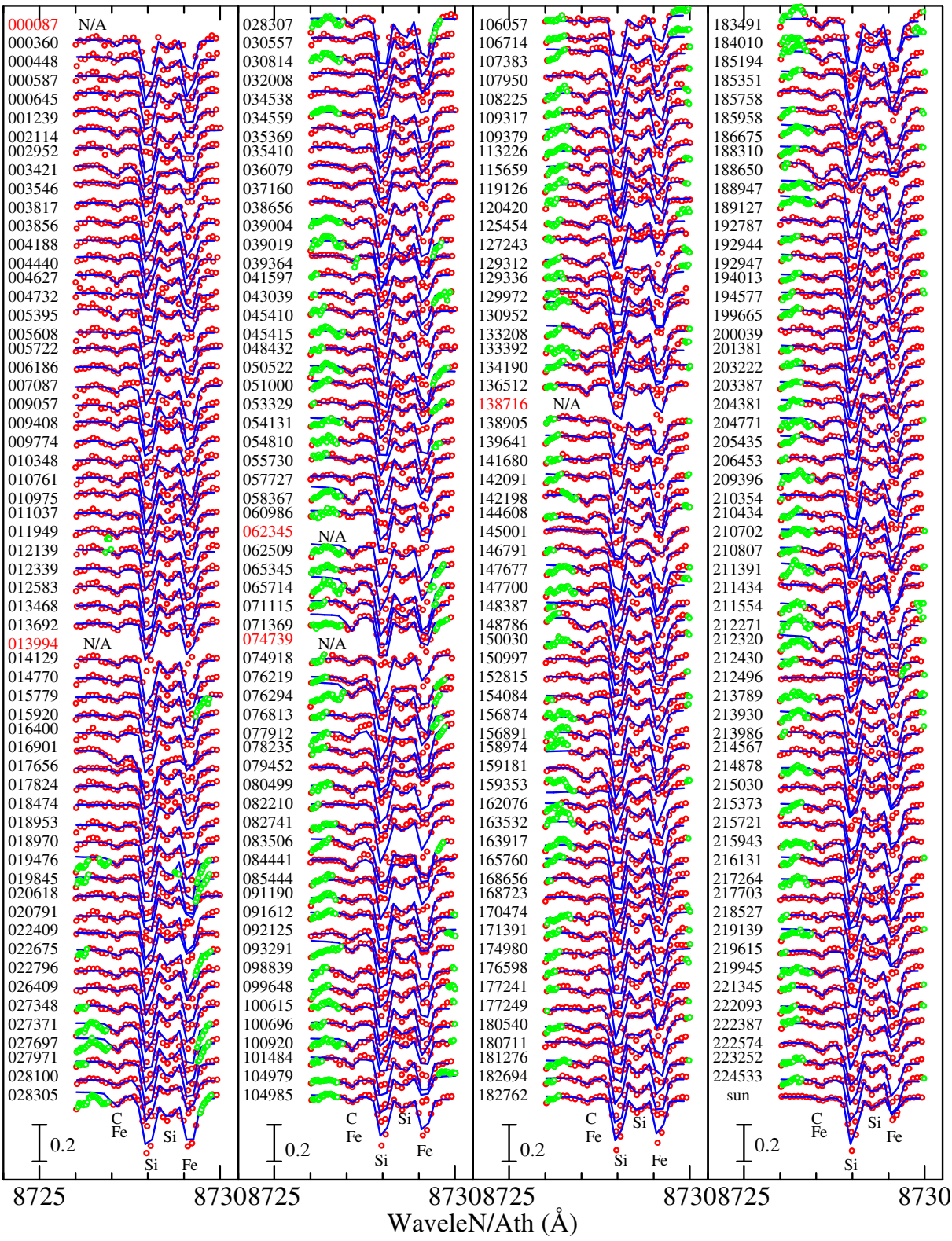

Fig. 5. Synthetic spectrum fitting in the 8726–8730 Å region comprising the [C I] (+ Fe I) 8727 line. Otherwise, the same as in figure 3, except that the applied vertical offset for each spectrum is 0.1 (instead of 0.2).

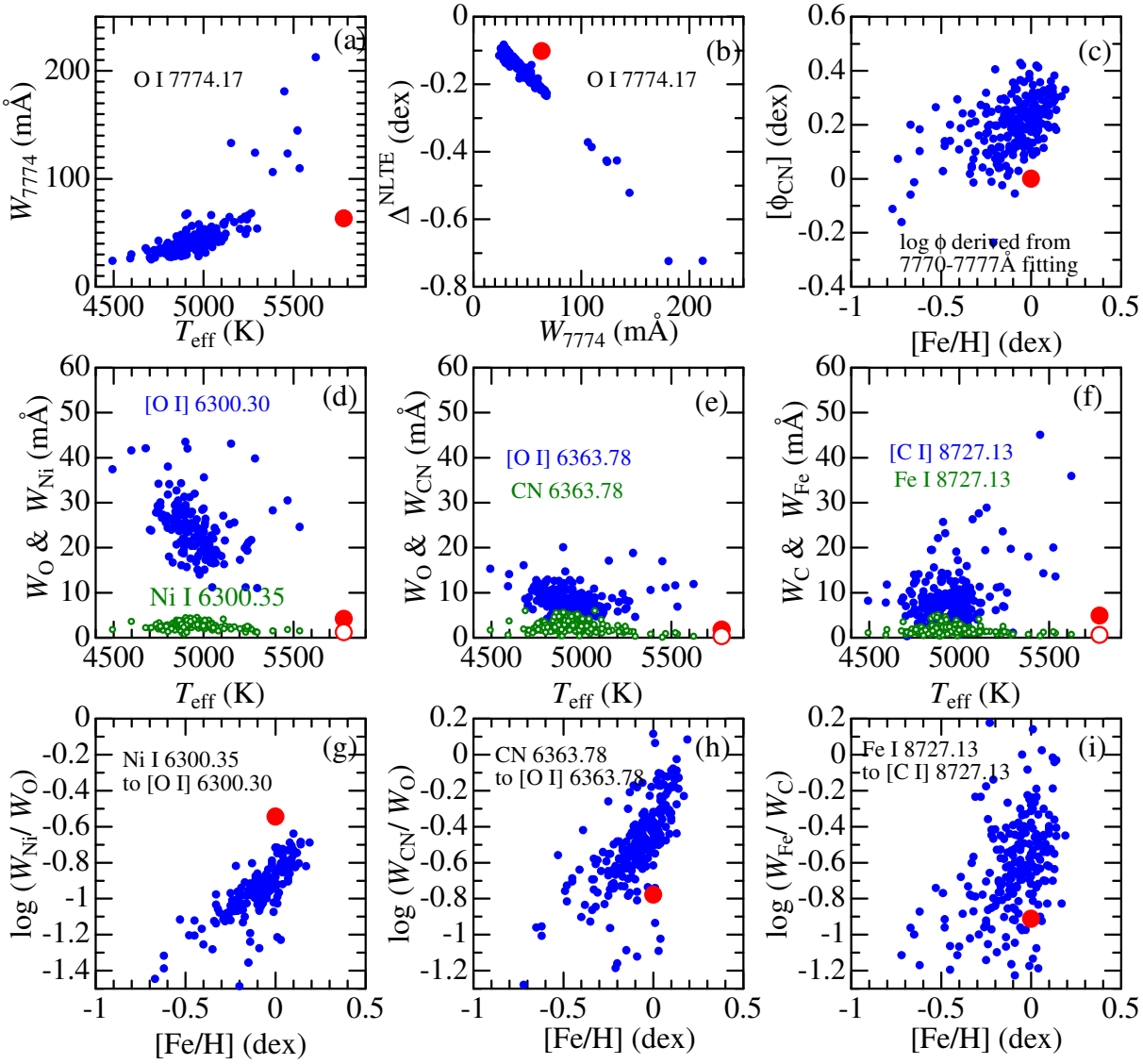

Fig. 6. Characteristics and behaviors of the quantities related to our abundance determinations. (a) W_{7774} vs. $T_{\rm eff}$, (b) $\Delta^{\rm NLTE}_{7774}$ vs. W_{7774}, (c) $[\phi_{\rm CN}]$ ($\equiv \log\phi_* - \log\phi_\odot$) vs. [Fe/H], (d) W_{6300}([O I] or Ni I) vs. $T_{\rm eff}$, (e) W_{6363}([O I] or CN) vs. $T_{\rm eff}$, (f) W_{8727}([C I] or Fe I) vs. $T_{\rm eff}$, (g) $\log(W_{\rm Ni6300}/W_{\rm O6300})$ vs. [Fe/H], (h) $\log(W_{\rm CN6363}/W_{\rm O6363})$ vs. [Fe/H], and (i) $\log(W_{\rm Fe8727}/W_{\rm C8727})$ vs. [Fe/H]. The solar values are indicated by large red circles.

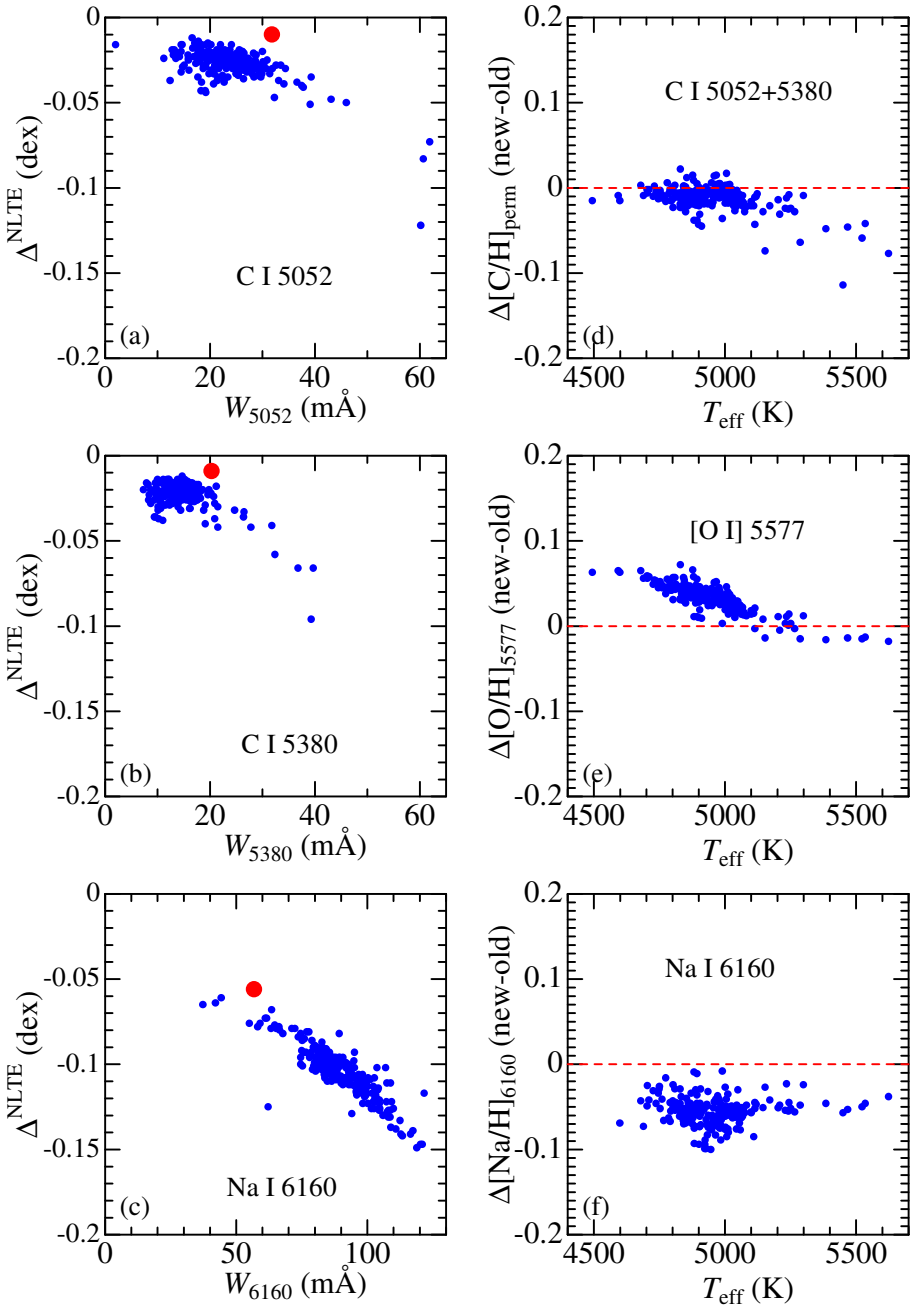

Fig. 7. Quantities related to our reanalysis of the equivalent widths measured in Paper I. Left panels (a, b, c): W_λ-dependence the non-LTE corrections for C I 5052, C I 5380, and Na I 6160 lines, where the results for the sun are represented by large red circles. Right panels (d, e, f): difference of the new [C/H]$_{5052/5380}$, [O/H]$_{5577}$, and [Na/H]$_{6160}$ (relative to the previous values published in Paper I) plotted against $T_{\rm eff}$.

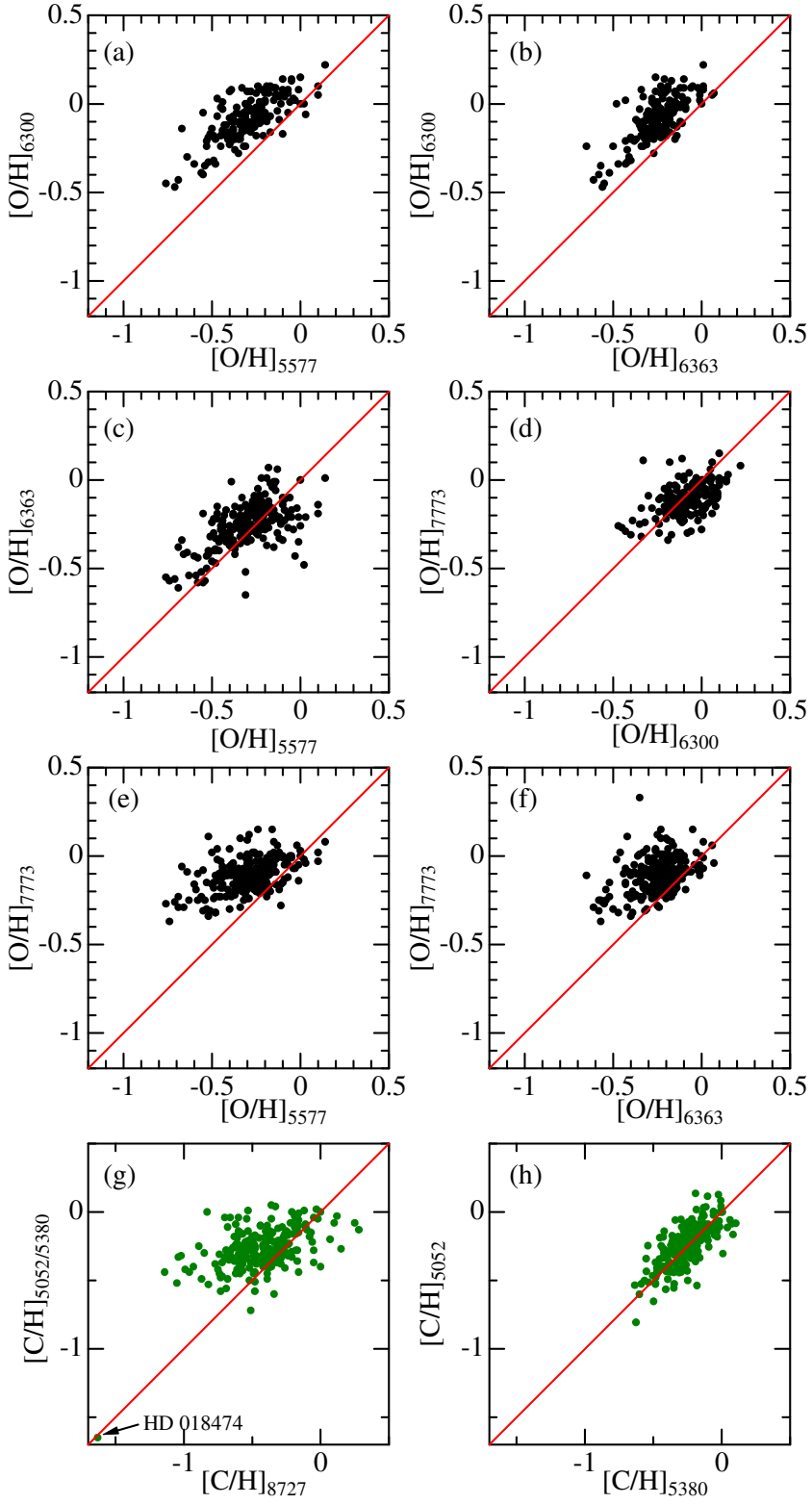

Fig. 8. Comparison of the various [O/H] results (as well as [C/H]) derived from different lines. (a) $[O/H]_{6300}$ vs. $[O/H]_{5577}$, (b) $[O/H]_{6300}$ vs. $[O/H]_{6363}$, (c) $[O/H]_{6363}$ vs. $[O/H]_{5577}$, (d) $[O/H]_{7773}$ vs. $[O/H]_{6300}$, (e) $[O/H]_{7773}$ vs. $[O/H]_{5577}$, (f) $[O/H]_{7773}$ vs. $[O/H]_{6363}$, (g) $[C/H]_{5052/5380}$ vs. $[C/H]_{8727}$, and (h) $[C/H]_{5052}$ vs. $[C/H]_{5380}$.

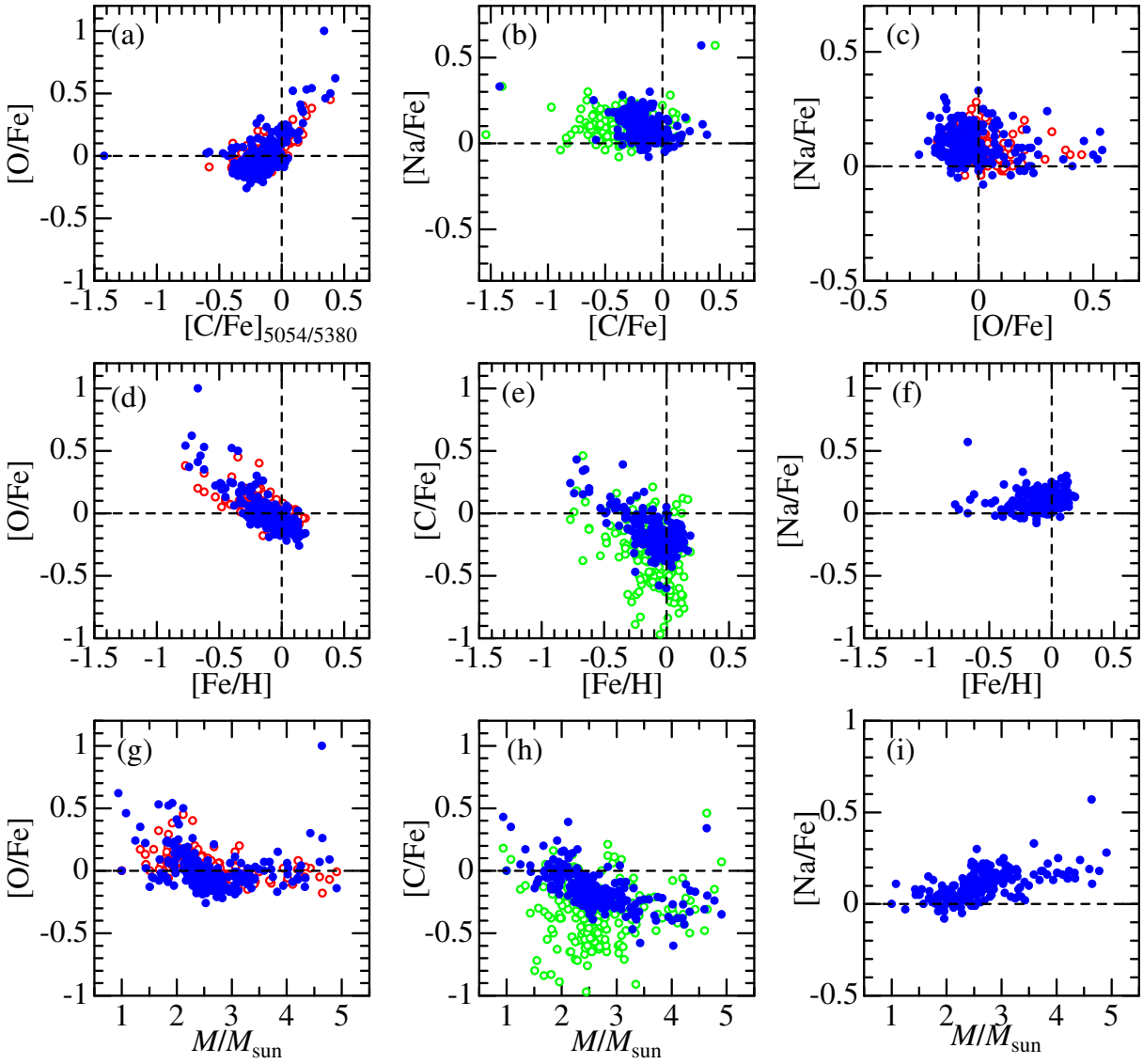

Fig. 9. Comparisons between [O/Fe] (from O I 7771–5 or [O I 6300), [C/Fe] (from C I 5052/5380 or [C I] 8727), and [Na/Fe] (from Na I 6160) with each other, and their relations to [Fe/H] as well as M. (a) [O/Fe] (7771–5 or 6300) vs. [C/Fe] (5052/5380), (b) [Na/Fe] vs. [C/Fe] (5052/5380 or 8727), (c) [Na/Fe] vs. [O/Fe] (7771–5 or 6300), (d) [O/Fe] (7771–5 or 6300) vs. [Fe/H], (e) [C/Fe] (5052/5380 or 8727) vs. [Fe/H], (f) [Na/Fe] vs. [Fe/H], (g) [O/Fe] (7771–5 or 6300) vs. M, (h) [C/Fe] (5052/5380 or 8727) vs. M, and (j) [Na/Fe] vs. M. The results from forbidden lines are shown in open symbols in panels (a), (b), (c), (d), (e), (g), and (h), while those from permitted lines are in filled symbols.

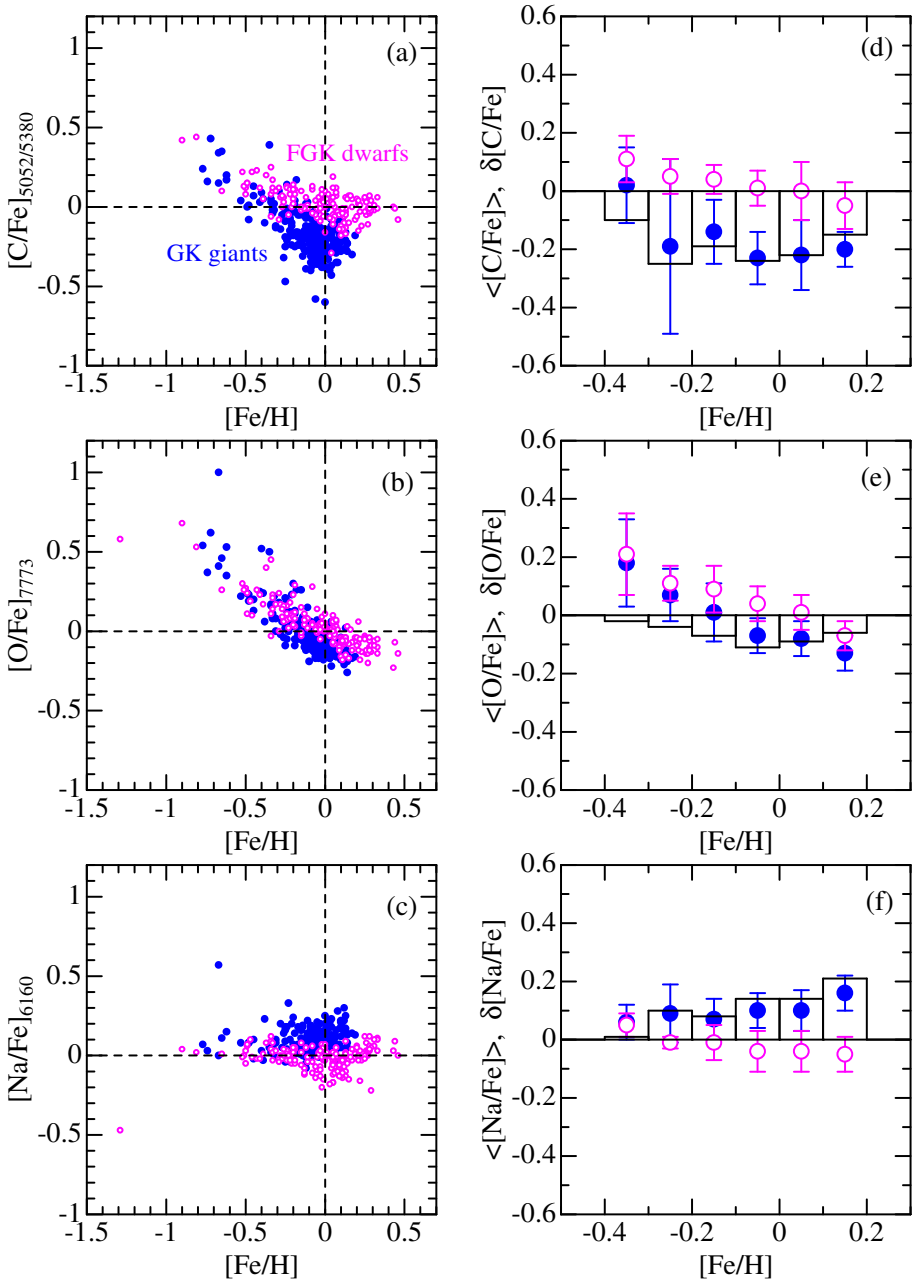

Fig. 10. Left-hand panels show the comparison of [X/Fe] vs.[Fe/H] relations (X = C or O or Na; based on permitted lines of C I 5052/5380, O I 7771–5, and Na I 6160) derived in this study for 239 G–K giants (filled symbols) with those of 160 FGK dwarfs (open symbols) published by Takeda and Honda (2005) (for C and O) and Takeda (2007) (for Na). Symbols in the right-side panels give the mean $\langle$[X/Fe]$\rangle$ at each metallicity group (0.1 dex bin within $-0.4 \leq$ [Fe/H] $\leq +0.2$) where error bars denote the standard deviations, while bar graphs represent the mean abundance differences between giants and dwarfs defined as $\langle$[X/Fe]$\rangle_{\rm giants} - \langle$[X/Fe]$\rangle_{\rm dwarfs}$. Panels (a)/(d), (b)/(e), and (c)/(f) correspond to C, O, and Na, respectively.

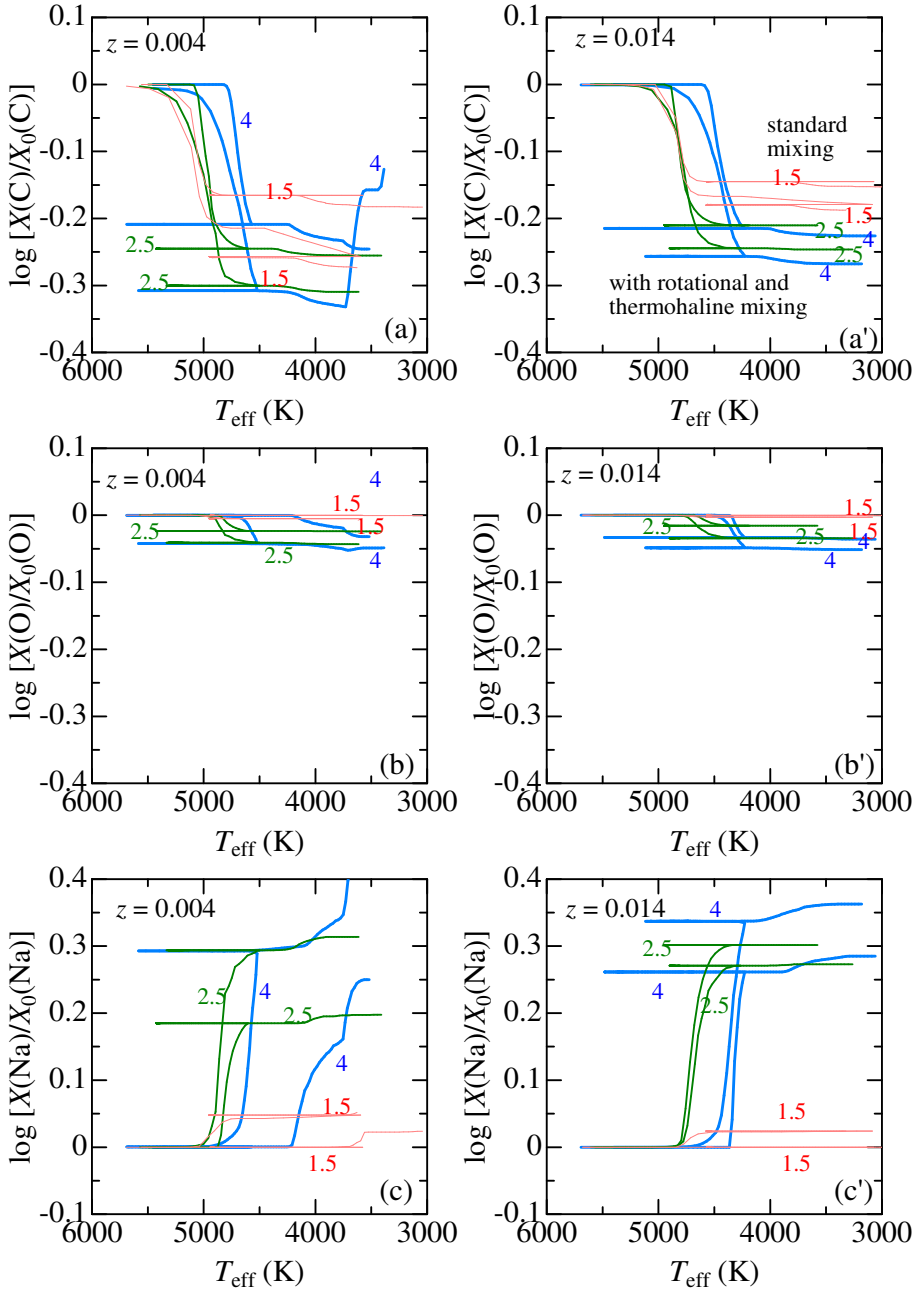

Fig. 11. Lagarde et al.'s (2012) theoretically simulated $\log[X/X_0]$ (logarithmic mass fraction ratio of the relevant element at the surface relative to the initial value) plotted against $T_{\rm eff}$, where top, middle, and bottom panels are for C (= ^{12}C+^{13}C+^{14}C $\simeq^{12}$C), O (= ^{16}O+^{17}O+^{18}O $\simeq^{16}$O), and Na (=^{23}Na), respectively. The left panels are for $z = 0.04$ (0.3× solar metallicity) and the right are for $z = 0.14$ (1× solar metallicity). The results corresponding to three stellar masses of 1.5, 2.5, and 4.0 $M_\odot$ are shown here, which are discriminated by line thickness (thin orange line, normal green line, and thick blue lines, respectively). Here, we restricted the data only to those of the well-evolved red-giant stage satisfying the conditions of $T_{\rm eff} < 5700$ K and $age > 10^{7.5}$ yr. Note that two kinds of curves are shown corresponding to different treatments of envelope mixing; i.e., standard treatment and treatment including rotational and thermohaline mixing. Although these two sets are drawn in the same line-type, they are discernible as the latter generally shows larger anomaly (and the appearance of peculiarity tends to begin earlier; i.e., at higher $T_{\rm eff}$) as compared to the former.